AGU ADVANCING EARTH AND SPACE SCIENCES

Geophysical Research Letters

RESEARCH LETTER
10.1029/2024GL113502

Radiation Belt Electron Acceleration Inside the Plasmasphere

Man Hua[1] **and Jacob Bortnik**[1]

[1]Department of Atmospheric and Oceanic Sciences, UCLA, Los Angeles, CA, USA

Key Points:

- We report a new population of outer belt electron acceleration events from 300 keV to ∼1.5 MeV observed inside the plasmasphere (IE)
- At >300 keV, the IEs are weaker but occur more frequently compared to the stronger acceleration events observed outside the plasmasphere
- The evolution of electron phase space density of a typical IE shows monotonically increasing radial profile, suggesting the crucial role of radial transport

Supporting Information:

Supporting Information may be found in the online version of this article.

Correspondence to:

M. Hua,
manhua@ucla.edu

Citation:

Hua, M., & Bortnik, J. (2025). Radiation belt electron acceleration inside the plasmasphere. *Geophysical Research Letters*, *52*, e2024GL113502. https://doi.org/10.1029/2024GL113502

Received 7 NOV 2024
Accepted 12 FEB 2025

Abstract We report a new population of outer belt electron acceleration events ranging from hundreds of keV to ∼1.5 MeV that occurred inside the plasmasphere, which we named "Inside Events" (IEs). Based on 6 year observations from Van Allen Probes, we compare the statistical distributions of IEs with electron acceleration events outside the plasmasphere (OEs). We find that most IEs were observed at $L < 4.0$ at energies below ∼1.5 MeV, with weaker acceleration ratio (<10) and larger event numbers (peaking value reaching >200), compared to stronger but less frequently occurred (peaking event numbers only reaching ∼80) OEs that were mostly observed at $L > 4.0$. The evolution of electron phase space density of a typical IE shows signature of inward radial diffusion or transport. Our study provides a feasible mechanism for IE, which is the results of the inward radial transport of the electron acceleration in the outer region of outer belt.

Plain Language Summary Since the discovery of the Earth's Van Allen radiation belts in 1958, extensive studies have advanced our understanding of outer belt electron acceleration mechanisms. However, most previous studies focused on the electron acceleration process occurring in the low electron density region, outside the plasmasphere. Although limited previous studies reported the electron flux enhancements penetrated down to very low L-shells ($L = 2.5$), involving flux enhancements inside the plasmasphere, these studies did not specify the plasmapause location. In this letter, we report a new population of outer belt electron acceleration events ranging from hundreds of keV to ∼1.5 MeV observed inside the plasmasphere. The "inside electron acceleration events" (IEs) are weaker but occur much more frequently compared to the stronger acceleration events observed outside plasmasphere, and cannot be neglected when investigating radiation belt electron dynamics. The evolution of electron phase space density (PSD) of a typical IE event demonstrates signature of inward radial transport, showing gradual flux enhancements over several days and monotonically increasing radial profile of electron PSD. Our study provides convincing evidence that this observed IE in the low L-shell region ($L = 2.5$) was dominantly caused by inward radial transport of electron acceleration in the outer region of the outer belt.

1. Introduction

The acceleration mechanisms of Earth's radiation belt energetic electrons have been extensively studied since 1958 (W. Li & Hudson, 2019; Ripoll et al., 2020; Zheng et al., 2024). The acceleration of outer belt electrons, shown as electron flux enhancements by several orders of magnitude on timescales of hours to days (Baker et al., 2019), was demonstrated to be mainly caused by local acceleration due to whistler-mode chorus waves (e.g., Thorne et al., 2013) and/or inward radial diffusion (e.g., Hudson et al., 2008).

Whistler-mode chorus waves can efficiently accelerate "seed" electrons (100s keV) to relativistic energies (>1 MeV) in the low electron density region near the heart of the outer belt (Hua et al., 2022; Jaynes et al., 2015; Thorne et al., 2013), leading to growing local peaks observed in the radial profile of the electron phase space density (PSD) (Li, Ma, et al., 2016; Reeves et al., 2013). In contrast, inward radial diffusion results in a monotonically decreasing radial profile of electron PSD with decreasing L-shell (Jaynes et al., 2018; Ma et al., 2018; Tu et al., 2013). Inward radial diffusion is also important in redistributing electrons across L-shells once they have been accelerated locally by chorus waves (Zhao et al., 2019). While chorus waves can only accelerate electrons efficiently in the plasma trough that has low electron density (Allison et al., 2021; Summers et al., 1998), inward radial diffusion can accelerate electron both inside and outside the plasmasphere (Brautigam & Albert, 2000; Ozeke et al., 2014, 2018; O'Brien et al., 2016). Nevertheless, inward radial diffusion is more effective at higher L-shells having acceleration timescales of several orders of magnitude faster than those at lower L-shells (Ozeke et al., 2014; O'Brien et al., 2016).

It is noteworthy that there are other sources that may contribute to the electron acceleration in the radiation belts. While the Cosmic Ray Albedo Neutron Decay (CRAND) is believed to be the dominant source of >250 keV quasi-trapped electrons in the inner belt and slot region under quiet geomagnetic conditions, which is a relatively stable process, the contributions of CRAND are negligible at $L > 2$ during active times (Li et al., 2017; Zhang et al., 2019). Moreover, the substorm injections driven by interplanetary shocks can cause prompt significant flux enhancements of relativistic electrons in the low L-shell region (Friedel et al., 1996; Li et al., 1993). While the storm-time enhanced convection electric field can cause rapid electron injections at 10–100s keV (Liu et al., 2003; Su et al., 2016; Thorne et al., 2007), Mei et al. (2023) suggested that the >500 keV electrons are less affected by the convection electric field.

Despite many previous studies confirmed the importance of both local heating by chorus waves and inward radial diffusion in accelerating outer belt electrons, most of these studies focused on the electron acceleration observed outside the plasmapause in the low density region near the heart of the outer belt (e.g., Thorne et al., 2013). Furthermore, previous statistical studies demonstrated that the commencement of the electron flux enhancements occur predominantly outside of the innermost plasmapause location (Khoo et al., 2018, 2019). Although limited previous studies reported the electron flux enhancements penetrated down to very low L-shell (Claudepierre et al., 2017; Mei et al., 2024; Reeves et al., 2016; Zhao et al., 2017, 2023), involving flux enhancements inside the plasmasphere (Turner et al., 2017), these studies did not investigate the plasmapause location and their correlation with the observed electron acceleration.

In this letter, we report a new population of outer belt electron acceleration events that are observed to occur inside the plasmasphere at energies from 300 keV up to ~1.5 MeV based on 6 year measurements from Van Allen Probes. Our study, for the first time, compare the statistical distributions of inside electron acceleration events, which we named "Inside Events" (IEs), with the outside acceleration events (OEs). By analyzing the evolution of electron PSD during a typical IE event, we aim to provide a feasible mechanism to explain the underlying physical process of observed electron acceleration inside the plasmasphere down to $L = 2.5$.

2. Identification of Electron Acceleration Inside the Plasmasphere

In this study, we analyze all the electron acceleration events across energies of 300 keV–10 MeV over the region $L = 2.0 - 6.5$ using electron flux data from the Energetic Particle Composition and Thermal Plasma suite (ECT; Spence et al., 2013) onboard both Van Allen Probes (Mauk et al., 2013) during 2013–2018. The spin-averaged cross-calibrated fitted electron flux data product with high energy resolution is utilized (Boyd et al., 2019). The L-shell used in this study is the McIlwain L in TS04D model (Tsyganenko & Sitnov, 2005), from the magnetic ephemeris data provided by ECT team. We adopt similar method as Hua and Bortnik (2024) to automatically select acceleration events, but limited to acceleration events with monotonically increasing fluxes with time using the following criteria:

1. The electron fluxes are first binned into a 0.1 $L \times 6$ hr UT grid during 2013–2018.
2. An increase of flux by a factor of >5 compared to the fluxes observed anytime within a 2 day look-back time window is considered as one acceleration sample, which captures the quick and significant flux enhancements. Here, one acceleration sample corresponds to one acceleration point at a given L-shell and energy in one 6 hr time bin.
3. The acceleration samples at a given L-shell and energy that were observed within 1 day are considered as the same acceleration event.
4. The commencement of the acceleration event (t_0) is defined as the time of the lowest flux within 2 days of look-back window of the first acceleration sample, while the end of the event (t_1) corresponds to the time of flux reaching its maximum value. The acceleration ratio is the ratio of the flux at t_1 over the flux at t_0.
5. Only the events with monotonically increasing fluxes with time from t_0 to t_1 are selected in this study, which ensures the exclusion of the large oscillation of fluxes with time. There is no restriction on the time duration ($dt = t_1 - t_0$) when selecting the events.

To determine whether the identified acceleration events were IEs or OEs, we adopt the level-4 electron density data from the Electric and Magnetic Field Instrument Suite and Integrated Science (EMFISIS; Kletzing et al., 2013) instrument, which is inferred from the upper hybrid resonance frequency (Kurth et al., 2015). Based on previous studies (Li et al., 2010, 2016b), the satellite was assumed to be outside the plasmasphere when the electron density was either smaller than 50 cm^{-3} or the value from the empirical plasma trough density model

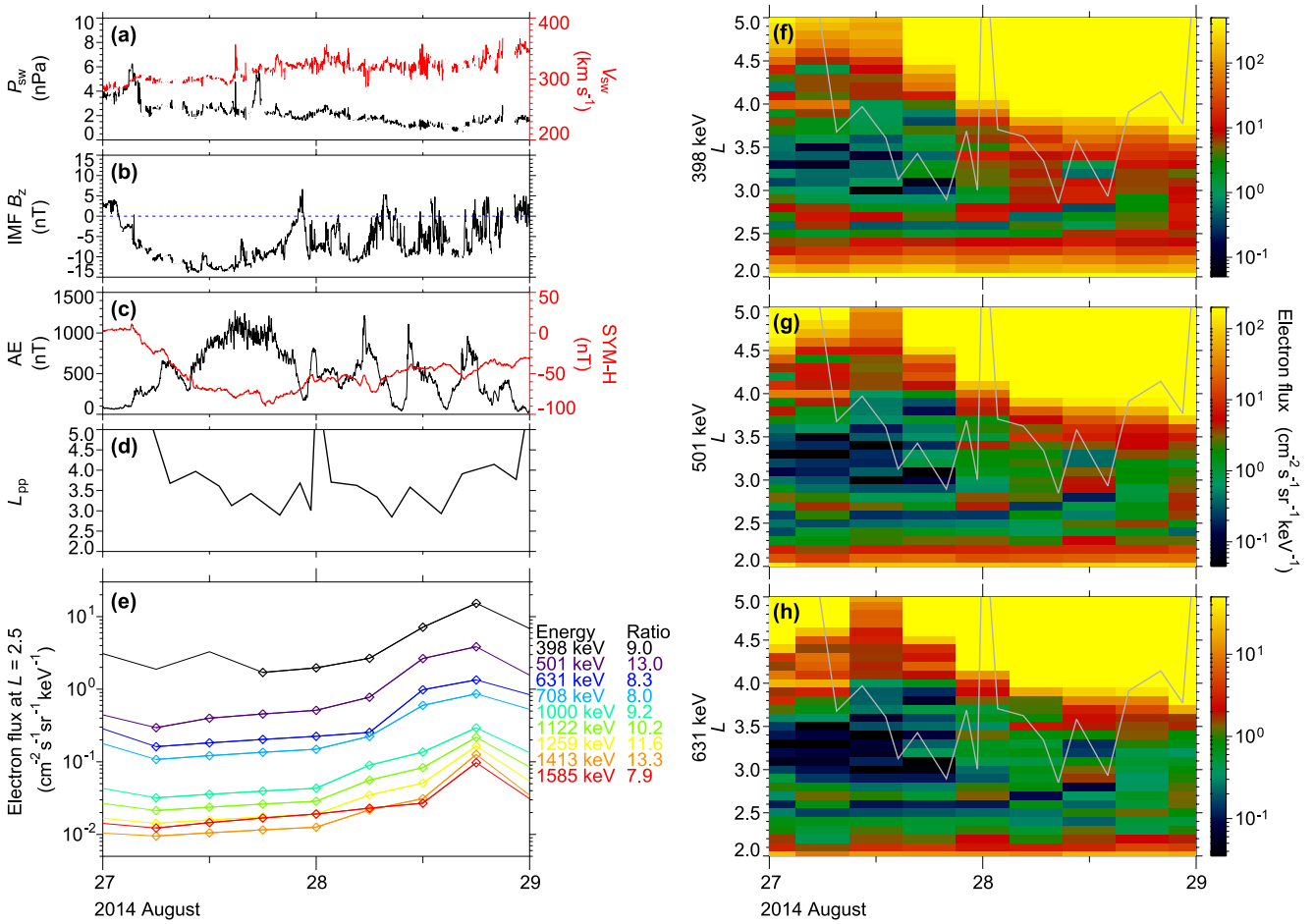

Figure 1. Examples of electron acceleration inside the plasmasphere observed by Van Allen Probes during 27–29 August 2014. (a) Solar wind pressure P_{sw} (black) and speed V_{sw} (red). (b) North-South component of the interplanetary magnetic field (IMF B_z) in Geocentric Solar Magnetospheric coordinate. (c) AE (black) and SYM-H (red) indices. (d) L-shell of the plasmapause location (L_{pp}). (e) Spin-averaged electron fluxes measured by ECT from both Van Allen Probes at $L = 2.5$ color-coded by energy, with the diamonds representing the identified acceleration events. The energies and acceleration ratio are marked on the left. (f)–(h) Spin-averaged electron fluxes at 398, 501, and 631 keV, respectively, with the over-plotted gray line showing the observed L_{pp}.

(Sheeley et al., 2001); otherwise, it was considered to be inside the plasmasphere. Hereafter, the IE means that the whole acceleration event was observed to be inside the plasmasphere, otherwise, it is considered as OE. The lowest L-shell where the satellite was outside the plasmasphere is recorded as the plasmapause location (L_{pp}) for each inbound and outbound satellite trajectory.

Figure 1 presents an overview of examples of IE events observed at energies from hundreds of keV to 1.5 MeV at $L = 2.5$ during 27–29 August 2014 (indicated by the diamond symbols in Figure 1e). This event was observed during active geomagnetic conditions, as indicated by the dynamic pressure pulse at ∼03:00 UT on 27 August and increasing solar wind velocity throughout the period (Figure 1a). There was a moderate geomagnetic storm with $(\text{SYM-H})_{min} \sim -90$ nT at ∼18:00 UT on 27 August and clusters of substorms (Figure 1c), likely triggered by a largely southward interplanetary magnetic field (Figure 1b). The observed L_{pp} remained above $L = 2.85$ during the whole event (Figure 1d), confirming that the electron acceleration at $L = 2.5$ (Figure 1e) was observed to be near the slot region and entirely inside the plasmasphere. Significant electron flux enhancements by ∼3 orders of magnitude were observed outside the plasmapause at $L >$ ∼4.0 (Figures 1f–1h), compared to the weak IE acceleration at $L = 2.5$ with acceleration ratio of ∼10. Figure S1 in Supporting Information S1 presents similar results but with a different color scheme to show more clearly the overall flux variations.

3. Results

3.1. Comparison of Statistical Properties of IEs and OEs

Figure 2 displays the comparison of the statistical properties in terms of event numbers (Figures 2a and 2b) and acceleration ratio (Figures 2c and 2d) for IEs (left column) and OEs (right column) as a function of L-shell and energy based on 6 year Van Allen Probes observations. The majority of the IEs concentrate in region below $L < 4.0$ at energies <2 MeV (Figure 2a), while the OEs were mostly observed at $L > 4.0$ at energies spanning from 300 keV to 5 MeV (Figure 2b). Although the IEs are mostly weak with acceleration ratio smaller than ∼10 compared to the much larger acceleration ratios reaching ∼200 for the OEs (Figures 2c and 2d), the IEs were much more frequently observed with the event numbers of >200 at $L \sim 2.5$ at ∼700 keV, compared to the largest outside acceleration event number only reaching ∼80 at hundreds of keV over $L = 4.0 - 5.0$ and at multi-MeV at $L > \sim 6.0$. These results also explain why there are two groups of electron acceleration events in our previous statistics (see Figure 2a in Hua & Bortnik, 2024), which were masked due to the mixing of IEs and OEs. Our results here directly demonstrate that the Group 1 events in our previous statistics are mostly IEs.

To facilitate comparison, we sort the acceleration events into 4 categories according to their acceleration ratio: weak ($5 \leq$ ratio < 10), moderate ($10 \leq$ ratio < 10 0), strong ($100 \leq$ ratio < 1000), and extreme strong (ratio ≥ 1000) acceleration events. The histogram of the number of the electron acceleration events divided in this way (Figures 2e–2l) again demonstrates that weak electron acceleration from 100s keV to 1.5 MeV is frequently observed inside the plasmasphere, whose event number is significantly larger than the OEs. Additionally, more IEs were observed at 631 and 794 keV compared to 398 keV over $L = 2.0 - 2.9$. Therefore, the weak but numerous IEs cannot be neglected when investigating radiation belt electron dynamics. Nevertheless, consistent with previous studies (Baker et al., 2019; Khoo et al., 2018, 2019), significant acceleration events were mostly observed at higher L-shells outside the plasmasphere albeit with a lower occurrence frequency. Moreover, the histogram of the time duration (dt) of the acceleration events is provided in Figure S2 in Supporting Information S1 with discussions given in Text S1 in Supporting Information S1. Most IEs have time duration less than 24 hr, consistent with Zhao et al. (2023) that most electron deep penetrations were fast.

3.2. Determining the Underlying Physical Processes

Investigating the evolution of the radial profile of electron PSD in the adiabatic invariant coordinate can help to unravel the underlying physical processes of electron acceleration (e.g., Reeves et al., 2013). We employ similar method as previous studies to calculate the electron PSD (Allison & Shprits, 2020; Li, Ma, et al., 2016; Turner et al., 2017). The Magnetic Ion Spectrometer (MagEIS; Blake et al., 2013) instrument onboard both Van Allen Probes provides back-ground-corrected electron flux data at energies from ∼30 keV to ∼4 MeV with pitch angle distribution (Claudepierre et al., 2019). Considering the similar method has been widely used in previous studies, the detailed calculation of electron PSD is provided in Text S2 in Supporting Information S1.

To reveal the potential underlying physical processes responsible for IEs, we analyze the evolution of the electron PSD during a typical IE that occurred during 26–29 August 2014 (Figure 3a), which is the same event shown in Figure 1. This is a relatively weak acceleration event with the acceleration ratio for hundreds of keV electrons at $L = 2.5$ remaining mostly below 10. Here, the selected $\mu = 30$ MeV/G and $K = 0.03$ $G^{0.5}R_E$ correspond to ∼500 keV electrons at $L^* = 2.5$, or ∼300 keV electrons at $L^* = 3.0$ (see Figure S3 in Supporting Information S1). The observed plasmapause location remained above $L = 2.85$ during the entire event (Figure 3c). The significant elevation of electron PSD occurred first at the outer belt at $L^* > \sim 3.2$ within ∼20 hr of commencement, leading to a sharp gradient in the radial profile of electron PSD (shown in light blue color). The resulting radial profile of electron PSD increased monotonically with increasing L^* showing no local peaks, consistent with the signature of acceleration through inward transport of electrons. Strong substorm activity during this time period (Figure 1c) can also cause rapid injections at the high L^* regions (Friedel et al., 1996; Su et al., 2016). Only after the acceleration occurred at $L^* > \sim 3.2$, the electron PSD at $L^* = 2.5 - 3.0$ gradually increased during 24–60 hr of this event (shown from light blue to red colors), exhibiting electron PSD monotonically increasing with increasing L^*. Meanwhile, the electron PSD at $L^* > \sim 3.7$ gradually decreased, leading to an overall flatter PSD radial gradient compared to the sharp radial gradient that was formed within first 20 hr. This trend of radial gradient becoming flatter at $L^* > \sim 3.7$ is consistent with Zhao et al. (2023). This overall evolution of electron PSD suggests that the electron acceleration inside the plasmasphere at the inner edge of the outer belt was the

10.1029/2024GL113502

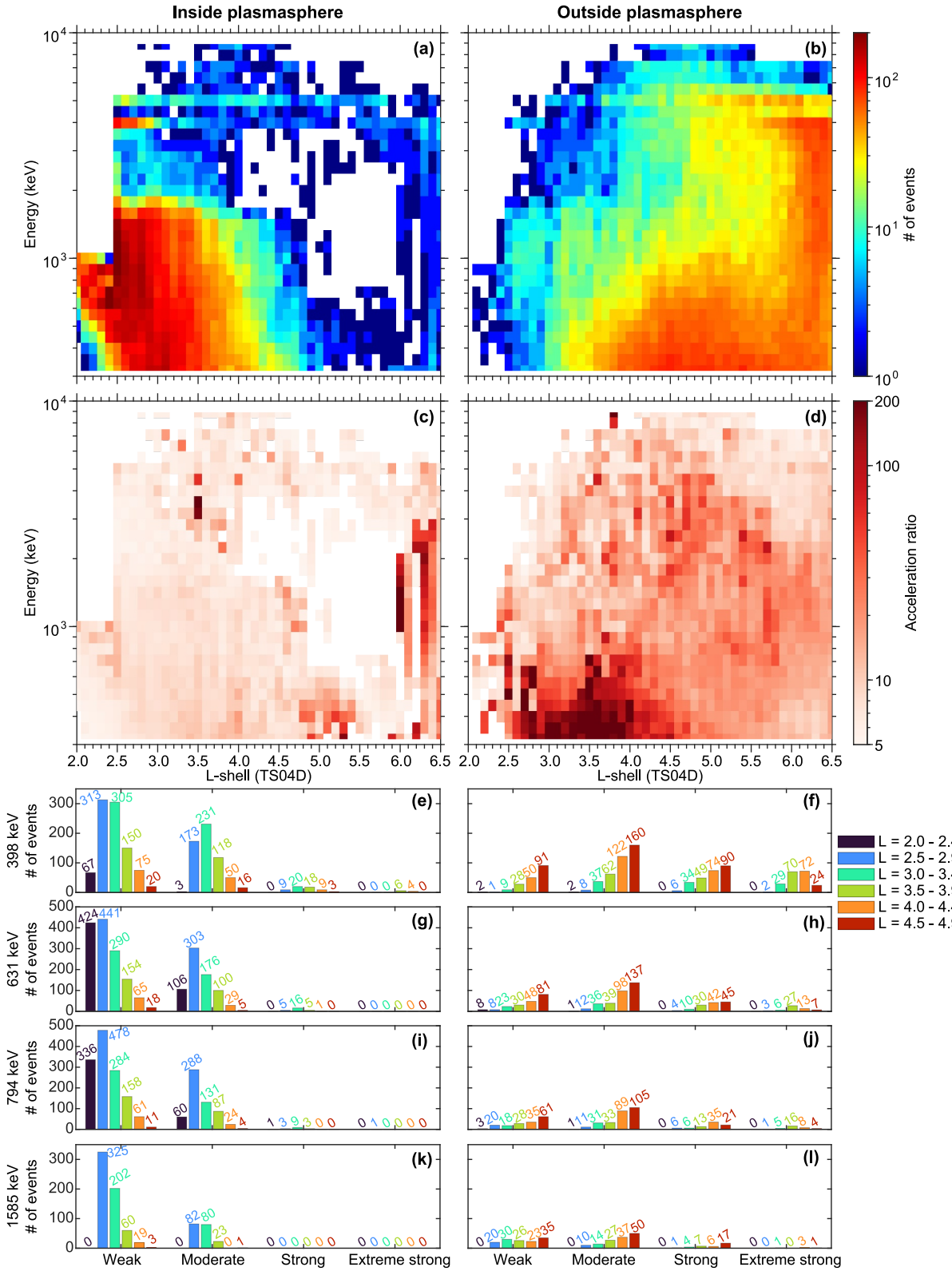

Figure 2. Comparison of statistical distributions of electron acceleration events observed inside (left column) and outside (right column) the plasmasphere based on Van Allen Probes observations during 2013–2018. Statistical distributions of (a–b) number of electron acceleration events. (c–d) median results of acceleration ratio as a function of L-shell and energy. (e–j) Histogram of the number of acceleration events that are categorized into weak ($5 \leq$ ratio < 10), moderate ($10 \leq$ ratio < 100), strong ($100 \leq$ ratio < 1000). extreme strong (ratio ≥ 1000) acceleration events at color-coded L-shells, with the corresponding event numbers marked on the top.

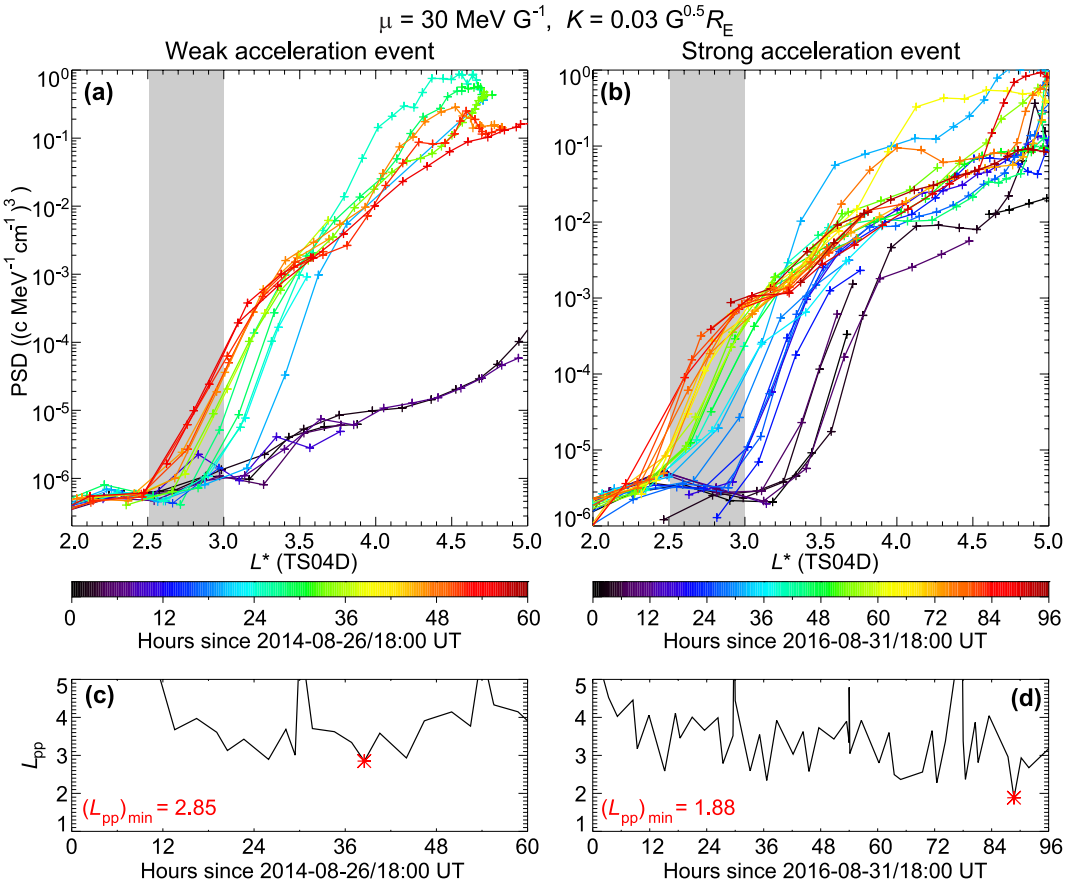

Figure 3. Comparison of electron phase space density (PSD) evolution during weak and strong electron acceleration events. Evolution of electron PSD at $\mu = 30$ MeV/G and $K = 0.03$ G$^{0.5}R_E$ as a function of L^* (calculated using TS04D) at color-coded times for (a) the weak IE during 26–29 August 2014, (b) the strong acceleration OE from 31 August to 4 September 2016. (c)–(d) The observed plasmapause location (L_{pp}) in each case, with the minimum L_{pp} during the whole event marked with a red star.

result of the gradual inward radial transport of the electron acceleration in the outer region of the outer belt, possibly by diffusive (Ozeke et al., 2014) or/and advective transport (Li et al., 2021).

For comparison, we perform a similar analysis of the electron PSD observed during a typical strong acceleration event (Figure 3b). For the strong acceleration event taking place from 31 August to 4 September 2016, the acceleration ratios for 100s keV electrons at $L = 2.5$ are mostly above 100 (not shown). The plasmapause location penetrated below $L = 2.5$ several times, with the lowest $L_{pp} = 1.88$ (Figure 3d). Similar to the weak acceleration event, the electron PSD during the strong acceleration event was first significantly elevated at $L^* > 3.0$ within ~1 day (shown from black to blue color in Figure 3b), resulting in a sharp gradient in the PSD radial profile. Due to the lower L_{pp} in the strong acceleration event, this quick electron PSD enhancement penetrated down to lower L^* compared to the weaker event, presumably still outside the nominal plasmapause. After the first acceleration of electrons at $L^* > 3.0$, the electron PSD at $L^* = 2.5 - 3.0$ gradually increased during ~24–96 hr of this event (shown from light blue to red colors), which smoothed the sharp gradient in the PSD radial profile. This acceleration process also shows monotonically increasing PSD radial profiles over $L^* = 2.5 - 3.0$, suggesting the important role of inward radial transport in such low L^* region. Meanwhile, the electron PSD near the heart of the outer belt at $L^* > 4.0$ was sustained without showing significant decrease, which can be provided by continuous substorm injections and/or inward radial transport of electrons from a source at higher L-shells. The stronger acceleration over $L^* = 2.5 - 3.0$ compared to the weak acceleration event in Figure 3a can be attributed to the sustained high levels of electron PSD in the outer belt, which guarantees the source for electron acceleration at $L^* = 2.5 - 3.0$ via inward radial transport. Similar results for higher μ from 50 to 200 MeV/G are provided in Figure S4 in Supporting Information S1, showing signature of inward radial transport at $L^* = 3.0 - 3.5$.

10.1029/2024GL113502

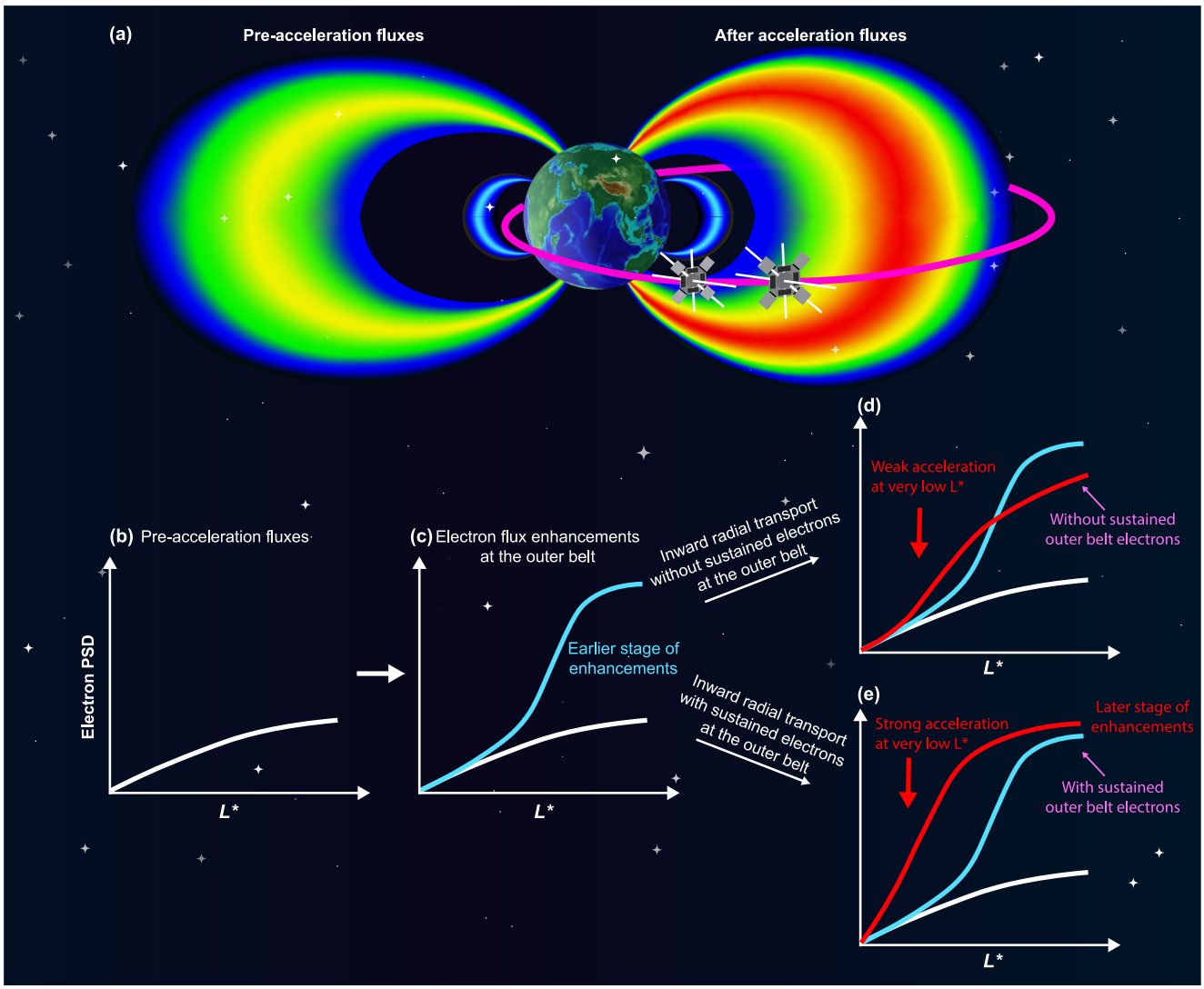

Figure 4. Schematic illustration of inward radial transport-driven radiation belt electron acceleration inside and outside the plasmasphere near the inner edge of the outer belt. (a) Electron fluxes before (left side) and after (right side) the acceleration event. (b)–(e) Multi-step processes required to accelerate electrons inside the plasmasphere by inward radial transport. (b) Radial profile of electron fluxes before acceleration. (c) Electron flux enhancement at the outer belt at high L^* region, with electron phase space density forming a sharp gradient. (d) Weak, and (e) strong electron acceleration at the inner edge of the outer belt as a result of the electron acceleration in the outer region of outer belt by inward radial transport without and with sustained electrons at the outer belt, respectively.

Figure 4 is a schematic illustration of inward radial transport-driven radiation belt electron acceleration inside and outside the plasmasphere near the slot and close to the inner edge of the outer belt. First, the electron acceleration occurs at the outer belt at high L^* region, forming a sharp gradient in the electron PSD radial profile. Then, inward radial transport tends to smooth this sharp gradient by transporting electrons at higher L^* to lower L^* region (possibly by diffusive or/and advective transport; Mei et al., 2023), resulting in the weak and strong electron acceleration close to the inner edge of the outer belt without and with sustained electrons at the outer belt, respectively. The strong acceleration events might be associated with slot refilling events (Thorne et al., 2007).

While other acceleration mechanisms can also contribute to the electron acceleration inside the plasmasphere, they are less likely to dominate this electron acceleration at this low L^* region shown in Figure 3 which were observed during active times for the following reasons: (a) The contributions from CRAND is negligible at $L > 2$ during geomagnetically active times (Zhang et al., 2019); (b) The electron PSD over $L^* = 2.5 - 3.0$ demonstrates the signature of a diffusive processes, that is, a gradually increasing of electron PSD over several days instead of a prompt elevation, which is less likely to be caused by sudden, direct substorm injections (Li

et al., 1993); (c) The acceleration events were observed from ~300 keV to ~1.5 MeV, which extends beyond the most efficient energy range of acceleration driven by the enhanced convection electric field (Mei et al., 2023). Considering all these factors, together with the signature of the inward radial transport from the electron PSD evolution, we believe that inward radial transport caused by diffusive (Ozeke et al., 2014) or/and advective (Li et al., 2021) processes is the most promising candidate mechanism to dominate this observed IE acceleration.

4. Conclusions and Discussions

Our study identifies a new population of outer belt electron acceleration events observed at energies from 300 keV to ~1.5 MeV, inside the plasmasphere, which we named IEs. The comparison of the statistical distributions of IEs with OEs demonstrates that the weaker IEs occur much more frequently than the stronger OEs. By analyzing the evolution of electron PSD in adiabatic coordinate during a typical IE event, our results provide solid evidence that the IE acceleration at the inner edge of the outer belt can be caused by the inward radial transport of the electron acceleration in the outer region of outer belt. Our major conclusions are as follows.

1. The majority of IEs were observed at $L < 4.0$ at energies from 300 keV to ~1.5 MeV, with weak acceleration ratio (mostly < 10) and large event numbers (e.g., reaching >200 at $L = 2.5$ at ~700 keV).
2. OEs were mostly observed at $L > 4.0$ at energies from 300 keV to 5 MeV, with strong acceleration ratio (mostly >10) and small event numbers (e.g., peaking value only reaching ~80 at hundreds of keV over $L = 4.0 - 5.0$ and at multi-MeV at $L > \sim 6.0$).
3. The evolution of electron PSD during a typical IE event demonstrates gradual flux enhancements over several days and monotonically increasing radial profiles, suggesting the dominant role of radial transport in accelerating electrons at $L^* \sim 2.5$ inside the plasmasphere during this event, which provides a feasible explanation for the IEs.

Our results demonstrate much more frequently observed IEs compared to OEs, one possible reason is that some electron acceleration events at lower L-shells were observed without concurrent observed acceleration of hundreds of keV electrons at higher L-shells (see examples in Figures S5 and S6 in Supporting Information S1). However, injected electrons at tens of keV that were observed at higher L-shells (e.g., at $L > \sim 4.5$, see Figures S6g–S6h in Supporting Information S1) can contribute to acceleration at hundreds of keV at lower L-shells through deep injections or radial transport, whose acceleration mechanism is left to the future study. Moreover, the OEs at $L > \sim 4.0$ require either local seed electrons (100s keV) for local heating by chorus waves (Hua et al., 2022; Jaynes et al., 2015), or seed electrons (100s keV) at higher L-shells for inward transport when the first and second adiabatic invariants are conserved (see electron energies across L^* at fixed first and second adiabatic invariants in Figure S7 in Supporting Information S1). However, the IEs at hundreds of keV at $L = 2.5$ can be more related to the injected electrons at tens of keV at higher L-shells (e.g., $L > \sim 5.0$, see Figure S7 in Supporting Information S1). Therefore, the fewer OEs at $L > 4.0$ compared to IEs at $L < \sim 3.0$ can be attributed to less frequently observed injections of hundreds of keV electrons compared to tens of keV electrons in the high L-shell region (Reeves et al., 2016).

We note some limitations and possible improvements of this study. First, there can be uncertainties in the plasmapause location that can vary with magnetic local time, whose observations were limited due to spatio-temporal coverage of satellites. Future study can incorporate machine-learning model of electron density (e.g., Chu et al., 2017) to obtain global plasmapause location. Second, future simulations are needed to quantify how the sustained electrons at higher L^*, and the PSD radial gradient affect the electron acceleration at lower L^*. Additionally, more IEs were observed at 631 and 794 keV compared to 398 keV over $L = 2.5 - 2.9$ (Figure 2), which is opposite to the lower energy electrons that are more frequently transported to lower L-shells (Reeves et al., 2016; Zhao & Li, 2013). Previous studies demonstrated more efficient radial diffusion for electrons at lower energies compared to higher energies at a given L-shell (Liu et al., 2016). Future studies are needed to comprehensively investigate additional acceleration mechanisms for IEs.

Data Availability Statement

The ECT data were obtained from https://rbsp-ect.newmexicoconsortium.org/data_pub/. The electron density data from the EMFISIS instrument onboard Van Allen Probes were obtained from http://emfisis.physics.uiowa.edu/Flight. The geomagnetic indices were obtained from the OMNI data set (https://omniweb.gsfc.nasa.gov/ow_

min.html). The source data used to produce figures in the present study are publicly available at (Hua & Bortnik, 2024b).

Acknowledgments
We acknowledge the Van Allen Probes mission, particularly the ECT team for providing the particle data and EMFISIS team for providing the electron density data. We acknowledge use of NASA/GSFC's Space Physics Data Facility's OMNIWeb service, and OMNI data. The authors gratefully acknowledge subgrant 1559841 to the University of California, Los Angeles, from the University of Colorado Boulder under NASA Prime Grant agreement 80NSSC20K1580 and NSF GEM award 2025706 and 2247255.

References

Allison, H. J., & Shprits, Y. Y. (2020). Local heating of radiation belt electrons to ultra-relativistic energies. *Nature Communications*, *11*(1), 4533. https://doi.org/10.1038/s41467-020-18053-z

Allison, H. J., Shprits, Y. Y., Zhelavskaya, I. S., Wang, D., & Smirnov, A. G. (2021). Gyroresonant wave-particle interactions with chorus waves during extreme depletions of plasma density in the Van Allen radiation belts. *Science Advances*, *7*(5), eabc0380. https://doi.org/10.1126/sciadv.abc0380

Baker, D. N., Hoxie, V., Zhao, H., Jaynes, A. N., Kanekal, S., Li, X., & Elkington, S. (2019). Multiyear measurements of radiation belt electrons: Acceleration, transport, and loss. *Journal of Geophysical Research: Space Physics*, *124*(4), 2588–2602. https://doi.org/10.1029/2018JA026259

Blake, J. B., Carranza, P. A., Claudepierre, S. G., Clemmons, J. H., Crain, W. R., Jr., Dotan, Y., et al. (2013). The Magnetic Electron Ion Spectrometer (MagEIS) instruments aboard the Radiation Belt Storm Probes (RBSP) spacecraft. *Space Science Reviews*, *179*(1–4), 383–421. https://doi.org/10.1007/s11214-013-9991-8

Boyd, A. J., Reeves, G. D., Spence, H. E., Funsten, H. O., Larsen, B. A., Skoug, R. M., et al. (2019). RBSP-ECT combined spin-averaged electron flux data product. *Journal of Geophysical Research: Space Physics*, *124*(11), 9124–9136. https://doi.org/10.1029/2019JA026733

Brautigam, D. H., & Albert, J. M. (2000). Radial diffusion analysis of outer radiation belt electrons during the October 9, 1990, magnetic storm. *Journal of Geophysical Research*, *105*(A1), 291–309. https://doi.org/10.1029/1999JA900344

Chu, X., Bortnik, J., Li, W., Ma, Q., Denton, R., Yue, C., et al. (2017). A neural network model of three-dimensional dynamic electron density in the inner magnetosphere. *Journal of Geophysical Research: Space Physics*, *122*(9), 9183–9197. https://doi.org/10.1002/2017ja024464

Claudepierre, S. G., O'Brien, T. P., Fennell, J. F., Blake, J. B., Clemmons, J. H., Looper, M. D., et al. (2017). The hidden dynamics of relativistic electrons (0.7-1.5 MeV) in the inner zone and slot region. *Journal of Geophysical Research: Space Physics*, *122*(3), 3127–3144. https://doi.org/10.1002/2016JA023719

Claudepierre, S. G., O'Brien, T. P., Looper, M. D., Blake, J. B., Fennell, J. F., Roeder, J. L., et al. (2019). A revised look at relativistic electrons in the Earth's inner radiation zone and slot region. *Journal of Geophysical Research: Space Physics*, *124*(2), 934–951. https://doi.org/10.1029/2018JA026349

Friedel, R. H. W., Korth, A., & Kremser, G. (1996). Substorm onsets observed by CRRES: Determination of energetic particle source regions. *Journal of Geophysical Research*, *101*(A6), 13137–13154. https://doi.org/10.1029/96JA00399

Hua, M., & Bortnik, J. (2024). Upper limit of outer belt electron acceleration and their controlling geomagnetic conditions: A comparison of storm and non-storm events. *Geophysical Research Letters*, *51*(13), e2024GL109612. https://doi.org/10.1029/2024GL109612

Hua, M., & Bortnik, J. (2024b). Radiation belt electron acceleration inside the plasmasphere [Dataset]. *Figshare*. https://doi.org/10.6084/m9.figshare.26218037.v1

Hua, M., Bortnik, J., & Ma, Q. (2022). Upper limit of outer radiation belt electron acceleration driven by whistler-mode chorus waves. *Geophysical Research Letters*, *49*(15), e2022GL099618. https://doi.org/10.1029/2022GL099618

Hudson, M. K., Kress, B. T., Mueller, H. R., Zastrow, J. A., & Blake, J. B. (2008). Relationship of the Van Allen radiation belts to solar wind drivers. *Journal of Atmospheric and Solar-Terrestrial Physics*, *70*(5), 708–729. https://doi.org/10.1016/j.jastp.2007.11.003

Jaynes, A. N., Ali, A. F., Elkington, S. R., Malaspina, D. M., Baker, D. N., Li, X., et al. (2018). Fast diffusion of ultrarelativistic electrons in the outer radiation belt: 17 march 2015 storm event. *Geophysical Research Letters*, *45*(20), 10874–10882. https://doi.org/10.1029/2018GL079786

Jaynes, A. N., Baker, D. N., Singer, H. J., Rodriguez, J. V., Loto'aniu, T. M., Ali, A. F., et al. (2015). Source and seed populations for relativistic electrons: Their roles in radiation belt changes. *Journal of Geophysical Research: Space Physics*, *120*(9), 7240–7254. https://doi.org/10.1002/2015JA021234

Khoo, L.-Y., Li, X., Zhao, H., Chu, X., Xiang, Z., & Zhang, K. (2019). How sudden, intense energetic electron enhancements correlate with the innermost plasmapause locations under various solar wind drivers and geomagnetic conditions. *Journal of Geophysical Research: Space Physics*, *124*(11), 8992–9002. https://doi.org/10.1029/2019JA027412

Khoo, L. Y., Li, X., Zhao, H., Sarris, T. E., Xiang, Z., Zhang, K., et al. (2018). On the initial enhancement of energetic electrons and the innermost plasmapause locations: Coronal mass ejection-driven storm periods. *Journal of Geophysical Research: Space Physics*, *123*(11), 9252–9264. https://doi.org/10.1029/2018JA026074

Kletzing, C. A., Kurth, W. S., Acuna, M., MacDowall, R. J., Torbert, R. B., Averkamp, T., et al. (2013). The electric and magnetic field instrument suite and integrated science (EMFISIS) on RBSP. *Space Science Reviews*, *179*(1–4), 127–181. https://doi.org/10.1007/s11214-013-9993-6

Kurth, W. S., De Pascuale, S., Faden, J. B., Kletzing, C. A., Hospodarsky, G. B., Thaller, S., & Wygant, J. R. (2015). Electron densities inferred from plasma wave spectra obtained by the Waves instrument on Van Allen Probes. *Journal of Geophysical Research: Space Physics*, *120*(2), 904–914. https://doi.org/10.1002/2014JA020857

Li, W., & Hudson, M. K. (2019). Earth's van allen radiation belts: From discovery to the van allen probes era. *Journal of Geophysical Research: Space Physics*, *124*(11), 8319–8351. https://doi.org/10.1029/2018JA025940

Li, W., Ma, Q., Thorne, R. M., Bortnik, J., Zhang, X. J., Li, J., et al. (2016). Radiation belt electron acceleration during the 17 March 2015 geomagnetic storm: Observations and simulations. *Journal of Geophysical Research: Space Physics*, *121*(6), 5520–5536. https://doi.org/10.1002/2016JA022400

Li, W., Santolik, O., Bortnik, J., Thorne, R. M., Kletzing, C. A., Kurth, W. S., & Hospodarsky, G. B. (2016b). New chorus wave properties near the equator from Van Allen Probes wave observations. *Geophysical Research Letters*, *43*(10), 4725–4735. https://doi.org/10.1002/2016GL068780

Li, W., Thorne, R. M., Bortnik, J., Nishimura, Y., Angelopoulos, V., Chen, L., et al. (2010). Global distributions of suprathermal electrons observed on THEMIS and potential mechanisms for access into the plasmasphere. *Journal of Geophysical Research*, *115*(A12), A00J10. https://doi.org/10.1029/2010JA015687

Li, X., Selesnick, R., Schiller, Q., Zhang, K., Zhao, H., Baker, D. N., & Temerin, M. A. (2017). Measurement of electrons from albedo neutron decay and neutron density in near-Earth space. *Nature*, *552*(7685), 382–385. https://doi.org/10.1038/nature24642

Li, X., Temerin, R. M., Wygant, J. R., Hudson, M. K., & Blake, J. B. (1993). Simulation of the prompt energization and transport of radiation belt particles during the March 24, 1991 SSC. *Geophysical Research Letters*, *20*(22), 2423–2426. https://doi.org/10.1029/93GL02701

Li, Z., Elkington, S., Hudson, M., Patel, M., Boyd, A., Wygant, J., et al. (2021). Modeling advective transport of radiation belt electrons. *Journal of Atmospheric and Solar-Terrestrial Physics*, *214*, 105509. https://doi.org/10.1016/j.jastp.2020.105509

Liu, S., Chen, M. W., Lyons, L. R., Korth, H., Albert, J. M., Roeder, J. L., et al. (2003). Contribution of convective transport to stormtime ring current electron injection. *Journal of Geophysical Research*, *108*(A10), 1372. https://doi.org/10.1029/2003JA010004

Liu, W., Tu, W., Li, X., Sarris, T., Khotyaintsev, Y., Fu, H., et al. (2016). On the calculation of electric diffusion coefficient of radiation belt electrons with in situ electric field measurements by THEMIS. *Geophysical Research Letters*, *43*(3), 1023–1030. https://doi.org/10.1002/2015GL067398

Ma, Q., Li, W., Bortnik, J., Thorne, R. M., Chu, X., Ozeke, L. G., et al. (2018). Quantitative evaluation of radial diffusion and local acceleration processes during GEM challenge events. *Journal of Geophysical Research: Space Physics*, *123*(3), 1938–1952. https://doi.org/10.1002/2017JA025114

Mauk, B. H., Fox, N. J., Kanekal, S. G., Kessel, R. L., Sibeck, D. G., & Ukhorskiy, A. (2013). Science objectives and rationale for the radiation belt storm Probes mission. *Space Science Reviews*, *179*(1–4), 3–27. https://doi.org/10.1007/s11214-012-9908-y

Mei, Y., Li, X., Zhao, H., Sarris, T., Khoo, L., Hogan, B., et al. (2023). On the energy-dependent deep (L < 3.5) penetration of radiation belt electrons. *Geophysical Research Letters*, *50*(10), e2022GL101921. https://doi.org/10.1029/2022GL101921

Mei, Y., Li, X., Zhao, H., Xiang, Z., Hogan, B., O'Brien, D., & Sarris, T. (2024). On the physical mechanisms driving the different deep penetration of radiation belt electrons and protons. *Journal of Geophysical Research: Space Physics*, *129*(8), e2024JA032634. https://doi.org/10.1029/2024JA032634

O'Brien, T. P., Claudepierre, S. G., Guild, T. B., Fennell, J. F., Turner, D. L., Blake, J. B., et al. (2016). Inner zone and slot electron radial diffusion revisited. *Geophysical Research Letters*, *43*(14), 7301–7310. https://doi.org/10.1002/2016GL069749

Ozeke, L. G., Mann, I. R., Murphy, K. R., Degeling, A. W., Claudepierre, S. G., & Spence, H. E. (2018). Explaining the apparent impenetrable barrier to ultra-relativistic electrons in the outer Van Allen belt. *Nature Communications*, *9*(1), 1844. https://doi.org/10.1038/s41467-018-04162-3

Ozeke, L. G., Mann, I. R., Murphy, K. R., Jonathan Rae, I., & Milling, D. K. (2014). Analytic expressions for ULF wave radiation belt radial diffusion coefficients. *Journal of Geophysical Research: Space Physics*, *119*(3), 1587–1605. https://doi.org/10.1002/2013JA019204

Reeves, G. D., Friedel, R. H. W., Larsen, B. A., Skoug, R. M., Funsten, H. O., Claudepierre, S. G., et al. (2016). Energy-dependent dynamics of keV to MeV electrons in the inner zone, outer zone, and slot regions. *Journal of Geophysical Research: Space Physics*, *121*(1), 397–412. https://doi.org/10.1002/2015JA021569

Reeves, G. D., Spence, H. E., Henderson, M. G., Morley, S. K., Friedel, R. H. W., Funsten, H. O., et al. (2013). Electron acceleration in the heart of the Van Allen radiation belts. *Science*, *341*(6149), 991–994. https://doi.org/10.1126/science.1237743

Ripoll, J.-F., Claudepierre, S. G., Ukhorskiy, A. Y., Colpitts, C., Li, X., Fennell, J., & Crabtree, C. (2020). Particle dynamics in the earth's radiation belts: Review of current research and open questions. *Journal of Geophysical Research: Space Physics*, *125*(5), e2019JA026735. https://doi.org/10.1029/2019JA026735

Sheeley, B. W., Moldwin, M. B., Rassoul, H. K., & Anderson, R. R. (2001). An empirical plasmasphere and trough density model: CRRES observations. *Journal of Geophysical Research*, *106*(A11), 25631–25641. https://doi.org/10.1029/2000JA000286

Spence, H. E., Reeves, G. D., Baker, D. N., Blake, J. B., Bolton, M., Bourdarie, S., et al. (2013). Science goals and overview of the radiation belt storm probes (RBSP) energetic particle, composition, and thermal plasma (ECT) suite on NASA's Van Allen Probes mission. *Space Science Reviews*, *179*(1–4), 311–336. https://doi.org/10.1007/s11214-013-0007-5

Su, Y.-J., Selesnick, R. S., & Blake, J. B. (2016). Formation of the inner electron radiation belt by enhanced large-scale electric fields. *Journal of Geophysical Research: Space Physics*, *121*(9), 8508–8522. https://doi.org/10.1002/2016JA022881

Summers, D., Thorne, R. M., & Xiao, F. (1998). Relativistic theory of wave-particle resonant diffusion with application to electron acceleration in the magnetosphere. *Journal of Geophysical Research*, *103*(A9), 20487–20500. https://doi.org/10.1029/98JA01740

Thorne, R. M., Li, W., Ni, B., Ma, Q., Bortnik, J., Chen, L., et al. (2013). Rapid local acceleration of relativistic radiation-belt electrons by magnetospheric chorus. *Nature*, *504*(7480), 411–414. https://doi.org/10.1038/nature12889

Thorne, R. M., Shprits, Y. Y., Meredith, N. P., Horne, R. B., Li, W., & Lyons, L. R. (2007). Refilling of the slot region between the inner and outer electron radiation belts during geomagnetic storms. *Journal of Geophysical Research*, *112*(A6), A06203. https://doi.org/10.1029/2006JA012176

Tsyganenko, N. A., & Sitnov, M. I. (2005). Modeling the dynamics of the inner magnetosphere during strong geomagnetic storms. *Journal of Geophysical Research*, *110*(A3), A03208. https://doi.org/10.1029/2004JA010798

Tu, W., Cunningham, G. S., Chen, Y., Henderson, M. G., Camporeale, E., & Reeves, G. D. (2013). Modeling radiation belt electron dynamics during GEM challenge intervals with the DREAM3D diffusion model. *Journal of Geophysical Research: Space Physics*, *118*(10), 6197–6211. https://doi.org/10.1002/jgra.50560

Turner, D. L., O'Brien, T. P., Fennell, J. F., Claudepierre, S. G., Blake, J. B., Jaynes, A. N., et al. (2017). Investigating the source of near-relativistic and relativistic electrons in Earth's inner radiation belt. *Journal of Geophysical Research: Space Physics*, *122*(1), 695–710. https://doi.org/10.1002/2016JA023600

Zhang, K., Li, X., Zhao, H., Schiller, Q., Khoo, L.-Y., Xiang, Z., et al. (2019). Cosmic Ray Albedo Neutron Decay (CRAND) as a source of inner belt electrons: Energy spectrum study. *Geophysical Research Letters*, *46*(2), 544–552. https://doi.org/10.1029/2018GL080887

Zhao, H., Baker, D. N., Califf, S., Li, X., Jaynes, A. N., Leonard, T., et al. (2017). Van Allen probes measurements of energetic particle deep penetration into the low L region (L < 4) during the storm on 8 April 2016. *Journal of Geophysical Research: Space Physics*, *122*(12), 12140–12152. https://doi.org/10.1002/2017JA024558

Zhao, H., Baker, D. N., Li, X., Malaspina, D. M., Jaynes, A. N., & Kanekal, S. G. (2019). On the acceleration mechanism of ultrarelativistic electrons in the center of the outer radiation belt: A statistical study. *Journal of Geophysical Research: Space Physics*, *124*(11), 8590–8599. https://doi.org/10.1029/2019JA027111

Zhao, H., Califf, S. T., Goyal, R., Li, X., Gkioulidou, M., Manweiler, J. W., & Krantz, S. (2023). Statistical analysis of the differential deep penetration of energetic electrons and protons into the low L region (L < 4). *Journal of Geophysical Research: Space Physics*, *128*(4), e2022JA031125. https://doi.org/10.1029/2022JA031125

Zhao, H., & Li, X. (2013). Modeling energetic electron penetration into the slot region and inner radiation belt. *Journal of Geophysical Research: Space Physics*, *118*(11), 6936–6945. https://doi.org/10.1002/2013JA019240

Zheng, Y., Jun, I., Tu, W., Shprits, Y., Kim, W., Matthiä, D., et al. (2024). Overview, progress and next steps for our understanding of the near-earth space radiation and plasma environment: Science and applications. *Advances in Space Research*. https://doi.org/10.1016/j.asr.2024.05.017

References From the Supporting Information

Chen, Y., Friedel, R. H. W., Henderson, M. G., Claudepierre, S. G., Morley, S. K., & Spence, H. (2014). REPAD: An empirical model of pitch angle distributions for energetic electrons in the Earth's outer radiation belt. *Journal of Geophysical Research: Space Physics*, *119*(3), 1693–1708. https://doi.org/10.1002/2013JA019431

Gannon, J. L., Li, X., & Heynderickx, D. (2007). Pitch angle distribution analysis of radiation belt electrons based on Combined Release and Radiation Effects Satellite Medium Electrons A data. *Journal of Geophysical Research*, *112*(A5), A05212. https://doi.org/10.1029/2005JA011565

Ni, B., Zou, Z., Gu, X., Zhou, C., Thorne, R. M., Bortnik, J., et al. (2015). Variability of the pitch angle distribution of radiation belt ultrarelativistic electrons during and following intense geomagnetic storms: Van Allen Probes observations. *Journal of Geophysical Research: Space Physics*, *120*(6), 4863–4876. https://doi.org/10.1002/2015JA021065

Shi, R., Summers, D., Ni, B., Fennell, J. F., Blake, J. B., Spence, H. E., & Reeves, G. D. (2016). Survey of radiation belt energetic electron pitch angle distributions based on the Van Allen Probes MagEIS measurements. *Journal of Geophysical Research: Space Physics*, *121*(2), 1078–1090. https://doi.org/10.1002/2015JA021724

Zhao, H., Li, X., Blake, J. B., Fennell, J. F., Claudepierre, S. G., Baker, D. N., et al. (2014). Peculiar pitch angle distribution of relativistic electrons in the inner radiation belt and slot region. *Geophysical Research Letters*, *41*(7), 2250–2257. https://doi.org/10.1002/2014GL059725

Zhao, H., Friedel, R. H. W., Chen, Y., Reeves, G. D., Baker, D. N., Li, X., et al. (2018). An empirical model of radiation belt electron pitch angle distributions based on Van Allen Probes measurements. *Journal of Geophysical Research: Space Physics*, *123*(5), 3493–3511. https://doi.org/10.1029/2018JA025277